Triple-cation perovskite/silicon tandem solar cell

Ašmontas S., Gradauskas J., Grigucevičienė A., Leinartas K., Lučun A., Mujahid M., Petrauskas K., Selskis A., Sužiedėlis A., Šilėnas A. and Širmulis E.

Center for Physical Sciences and Technology, Saulėtekio Avenue 3, 10257 Vilnius, Lithuania office@ftmc.lt

Abstract. A tandem solar cell consisting of perovskite cell overlaid upon silicon cell is a promising option for surpassing the Shockley–Queisser limit for single-junction solar cells. We investigate photovoltaic properties of a triple-cation perovskite/silicon four-terminal tandem solar cell composed of a semitransparent $Cs_{0.06}(MA_{0.17}FA_{0.83})_{0.94}Pb(I_{0.83}Br_{0.17})_3$ layer-based perovskite cell placed onto industrial n-type monocrystalline bifacial PERT silicon solar cell. The power-conversion efficiency of 26.6% achieved by us is one of the highest values among those reported for the four-terminal perovskite/silicon tandem solar cells.

1. Introduction

Ever-increasing demands for energy needs make it necessary to look for new ways of increasing the contribution of renewable energy sources into global power generation. One of the most promising and environmentally friendly energy sources is electricity generated by solar cells (SCs). Currently, near 90% of the SCs produced worldwide are from silicon [1, 2]. Power-conversion efficiency (PCE) of a single-junction SC reaches 27.6% thanks to a technology of thin passivating a-Si heterojunction intrinsic layers and inter-digitated back contacts on n-type silicon wafers [3]. The thermodynamic efficiency limit for a Si-based SC is around 29.8% for the real AM 1.5 solar spectrum [4]. This theoretical limit is extremely difficult to reach, although the experimental values of the PCE are now slowly approaching it. One of the reasons of the above challenge is associated with the fact that the solar photons with the energies higher than the forbidden energy gap create electron–hole pairs, and the excess energy is transmitted to photo-induced carriers, thus making them hot ones [5]. As a result, the hot-carrier photovoltage U_{hot} is induced across a cell. The polarity of U_{hot} is opposite to that of the classical photovoltage resulted from the electron–hole pair generation [6, 7]. Therefore, light-induced carrier heating reduces the efficiency of SCs. To diminish the influence of hot carriers on the photovoltage across p-n junction, one can use a multi-junction tandem SC [8]. The negative effect of hot carriers can also be considerably reduced by means of coating silicon SCs with thin perovskite layers absorbing high-energy photons [9].

A tandem SC may have different configurations. In two-terminal configuration, both SCs are monolithically integrated, so that a wide-bandgap cell is fabricated directly on a narrow-bandgap cell [10–15]. The two cells are electrically connected in series through a recombination layer or a tunnel junction [12]. The total output voltage of such a tandem is the sum of the voltages of the

individual cells. The two-terminal tandem SCs need not only good electrical connection between the top and bottom component cells but also require current matching, which complicates a relevant fabrication process and increases production costs [16, 17]. In four-terminal configuration, two cells are joined together mechanically, with a wide-bandgap cell being stacked onto a narrow-bandgap cell [18–21]. The cells operate electrically independently. The total power is the sum of the powers generated by each of the separate cells. The basic requirements for any configuration are the same: the top cell must be a good absorber of visible light and transparent to infrared light. A perovskite layer is the most suitable material for fabricating the top cells due to its excellent optoelectronic properties such as strong light absorption across the entire visible range enabling usage of thin perovskite films [21], high carrier mobility [23, 24], long carrier diffusion length [25], high defect tolerance [26], and long lifetime of generated charge carriers [27, 28].

Below we will deal with the details of fabrication of a semi-transparent triple-cation perovskite SC. We will also report on experimental studies of the structure and the optical properties of perovskite $Cs_{0.06}(MA_{0.17}FA_{0.83})_{0.94}Pb(I_{0.83}Br_{0.17})_3$ layers, as well as the photoelectric properties of perovskite/silicon tandem SCs.

2. Fabrication and characterization of perovskite cell

The methods and procedures suggested and detailed in Refs. [9, 29–31] were used to fabricate a perovskite cell suitable for our tandem SC. Glass substrates with the size 25×25 mm^2 coated by fluorine-doped tin oxide layer (TEC 10 (3.3 mm), Ossila, UK) were taken as a base of the top perovskite cell. Prior to formation of the cell, a ~ 5 mm-wide strip of fluorine-doped tin oxide layer was removed (etched) from one edge of a glass substrate. Zn powder and 4 M HCl solution were used for etching fluorine-doped tin oxide. Unless otherwise noted, these and the other precursors were from Sigma-Aldrich (MO, USA). After etching fluorine-doped tin oxide, the substrates were cleaned for 20 min with a 2% Helmanex solution in an ultrasonic bath (S40 H, Elmasonic, Germany). Then the substrates were thoroughly rinsed several times with deionized water and ultrasonicated in isopropanol during 20 min. Finally, the substrates were dried by compressed Ar flow and treated for ~ 5 min in a low-pressure oxygen plasma cleaner (Atto, Diener electronic GmbH + Co. KG, Germany).

A ~ 30 nm-thick layer of compact (dense) TiO$_2$ was formed on the substrates by spraying a solution composed of titanium diisopropoxide (bis) acetylacetonate (Ti (acac)$_2$OiPr$_2$) and isopropanol (1:9 vol. ratio) and then sintering it for 15 min at 450°C on a hotplate (PZ 28-3T Prazitherm, Gestigkeit GmbH, Germany). The sintered TiO$_2$-coated substrates were left on the hotplate for ~ 6 h for natural cooling. After this, a spin-coating method was used to deposit a 150–220 nm-thick layer of mesoporous TiO$_2$ on a compact TiO$_2$ layer. The mesoporous TiO$_2$ layer was grown using a 30-nm TiO$_2$ particle paste (Dyesol 30NRD/ethanol) diluted in ethanol to the 1:6 wt. ratio. 150 µL of the TiO$_2$ solution thus prepared was pipetted with an automatic pipette (Eppendorf Research Plus, Eppendorf AG) on a surface of the substrate placed on a centrifuge table (SPIN 150i POLOS, SPS-Europe B.V.). The following spinning program was used: 4,000 rpm for 20 s, with acceleration 2,000 rpm/s.

Mesoporous TiO$_2$ was formed by sintering the layer in a dry air for 30 min at 450°C. Then a sample was cooled down to 150°C and placed immediately into a glovebox (MBRAUN MB-10-G from M. Braun Inertgas-Systeme GMBH, Germany) with controlled atmosphere. The relative humidity ≤ 0.5 ppm of N$_2$ was continuously maintained. The perovskite structures were grown on mesoporous TiO$_2$ by a one-step precipitation method from the precursor solution prepared as described

above. A mixture of anhydrous N, N-dimethyl-formamide (DMF) and dimethylsulfoxide (DMSO) was used as a solvent, with the volume ratio of the components being equal to 4:1. The contents of the precursors in our DMF/DMSO mixture were as follows: $1.1 \div 1.3$ M of PbI_2, 0.2 M of PbBr, 1 M of formamidinium iodide (FAI) and 0.2 M of methylammonium bromide (MABr). Then Cs ions were added to the precursor solution. A 1.5 M CsI solution in DMSO was used as a source of Cs and the concentration of CsI in the precursor solution was equal to 6%. According to the literature, the solution of this composition can be used to form the perovskite $Cs_x(MA_{0.17}FA_{0.83})_{(1-x)}Pb(I_{0.83}Br_{0.17})_3$ compound [31].

Fig. 1. Architecture of our triple-cation perovskite/silicon tandem SC composed of a top perovskite cell and a bottom silicon cell (not to be scaled).

To deposit the perovskite layer on mesoporous TiO_2, the sample was placed on a centrifuge table, and 150 µL of the precursor solution was dropped with an Eppendorf pipette. Immediately after that, a two-step spin program was initiated. At the first step, spinning at 1,000 rpm for 10 s was applied, with the acceleration 200 rpm/s. The parameters of the second step were 6,000 rpm, 30 s and 1,000 rpm/s. Before ending the spin-coating program (~ 10 s), 150 µL of chlorobenzene was dropped on the surface of our sample to remove any residuals of the solution. The samples were then transferred from the centrifuge table on a hotplate (Isotemp Fisherbrand from Thermo Fisher Scientific, USA) and annealed in inert-gas atmosphere for 60 min at 100°C. After annealing and natural cooling for ~ 10 min, a hole transport layer covering the perovskite layer was formed. The samples were placed again on the centrifuge table, poured with 150 µL of 70 mM 2-*N*,2-*N*,2-*N'*,2-*N'*,7-*N*,7-*N*,7-*N'*,7-*N'*-octakis(4-methoxyphenyl)-9,9'-spirobi[fluorene]-2,2',7,7'-tetramine (Spiro-OMeTAD) solution. Then a proper spin-coating program was initiated immediately (4,000 rpm for 25 s, with the acceleration 2,000 rpm/s). Prior to this procedure, 17 µL of Li-bis(trifluoromethylsulfonyl)imide (Li-TFSI) salt in anhydrous acetonitrile and 28.8 µL of 4-tert-butylpyridine (TBP) solution were added to Spiro-OMeTAD solution. Li-TFSI concentration in the solvent was equal to 10 mg·mL^{-1}. 70 nm-thick Au contacts were deposited in a vacuum chamber of a thermal-evaporation equipment "VAKSIS PVD Vapor-5S_Th" (Vaksis R&D and Engineering, Ankara, Turkey) on the top of the hole transport layer and on the open side of the fluorine-doped tin oxide.

A scheme of our perovskite SC is shown in Fig. 1. To compose our perovskite/silicon tandem SC, an industrial (DS New Energy, China) *n*-type monocrystalline bifacial passivated emitter rear totally diffused silicon SC was used as a bottom cell (see Fig. 2). A boron diffused p$^+$ emitter was situated on its top surface to ensure electrical matching between the perovskite cell and the silicon cell.
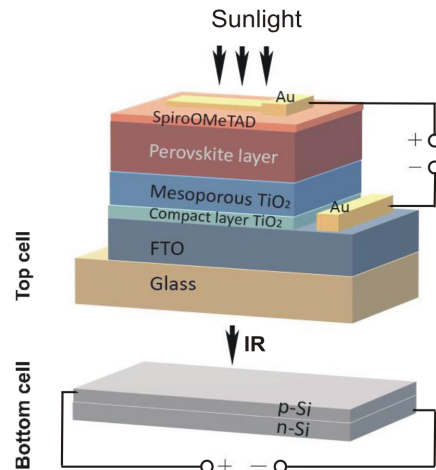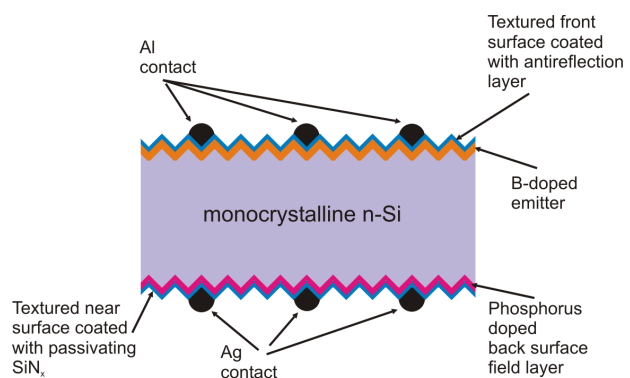

Fig. 2. Schematic cross-sectional view of a silicon SC used as a bottom cell of our perovskite/silicon tandem SC.

Photovoltaic characteristics of the perovskite SC were measured using a Keithley 2602A (Keithley Instruments Inc., Cleveland, USA) equipment. The 100 mW/cm^2 irradiance was achieved using an AM 1.5 spectral lamp (a Newport model 67005, Newport Corp., Irvine, USA), which was placed at a proper distance.

3. Results and discussion

Fig. 3a presents a top-view SEM image of our triple-cation perovskite film grown on the mesoporous titanium-dioxide layer. It is evident that the grain sizes are different. Some dimensions of the grains are larger than 1000 nm. The surfaces are flat and smooth, in agreement with the data reported elsewhere [32, 33]. A cross-sectional SEM image of the same perovskite film is shown in Fig. 3b. The thickness of the film is equal to (710 ± 40) nm. One can see that the film is composed of stacked grains not spanning the entire thickness of the layer.


400 nm   a)   500 nm   b)
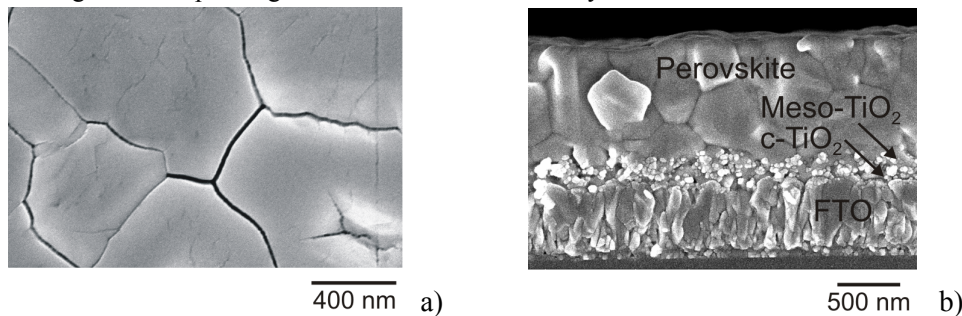
Fig. 3. Surface (a) and cross-sectional (b) SEM images of perovskite film grown on mesoporous titanium-dioxide layer.

The optical transmittance spectrum of the perovskite layer measured by us (see Fig. 4) testifies that this layer is a good absorber of visible light and remains semi-transparent in the infrared range. The transmittance is higher than 80% in the wavelength region 800–1100 nm.
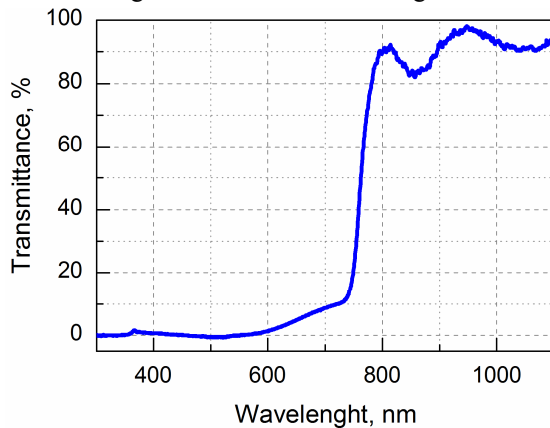
Fig. 4. Optical transmittance spectra of our triple-cation perovskite layer.

The experimental current–voltage characteristics of our triple-cation perovskite SC is depicted by red circles in Fig. 5. High enough short-circuit current density of the perovskite SC indicates a high quality of perovskite structure. The current–voltage characteristics of the silicon SC measured under the illumination 100 mW/cm^2 is also shown in Fig. 5 (blue triangles). The short-circuit current density of the separate silicon SC is higher than that of the perovskite SC. Note that the current–voltage characteristics of the bottom silicon cell in the tandem SC corresponds to green squares in Fig. 5. Finally, some photovoltaic parameters derived for our triple-cation perovskite SC (the open-circuit voltage V_{oc}, the short-current density J_{sc}, the fill factor
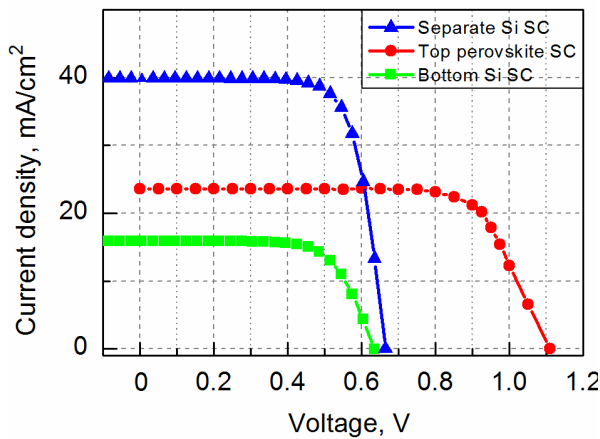
Fig. 5. Current–voltage characteristics of our triple-cation perovskite SC (red circles) and a silicon SC (blue triangles), as obtained under illumination 100 mW/cm². Green squares correspond to the current–voltage characteristics of Si cell placed below the perovskite SC in the tandem cell.

F and the PCE) are gathered in Table 1. A good optical transmittance and a high PCE of the semi-transparent triple-cation perovskite SC enables fabricating four-terminal tandem SCs basing on industrial silicon SC as a bottom cell.

Table 1. Some photovoltaic parameters of our perovskite SC, a separate silicon SC, and a silicon SC as a bottom cell in the tandem cell.

SC	V_{oc}, V	J_{sc}, mA·cm^{-2}	F, %	PCE, %
Top-perovskite	1.11	23.6	74	19.4
Separate-Si	0.67	40.0	72	19.3
Bottom-Si	0.64	15.8	71	7.2

When the perovskite SC is placed onto the silicon SC, the short-circuit current density of the latter drops down since most of the short-wavelength photons are absorbed in the top perovskite layer, and only a portion of the near-infrared photons can reach the bottom Si cell. The open-circuit voltage V_{oc} for the bottom cell is slightly lower than that of the separate silicon SC under the same illumination. The PCE of the bottom silicon SC in the tandem cell amounts to 7.2%. As a result, adding 19.4% corresponding to the top semi-transparent perovskite cell yields in the total 26.6% PCE of the four-terminal perovskite/silicon tandem SC, which is much higher than the efficiency of each separate subcell. The total PCE of our four-terminal perovskite/silicon tandem SC is higher than the value 25.2%, which has been achieved for the fully textured monolithic perovskite/silicon tandem SC [17]. It is close to the efficiency typical for the monolithic perovskite/silicon tandem SC with the nanocrystalline Si oxide interlayer [34]. Still, the parameter reported in the present work is higher than the value 15.15% reported in Ref. [35] for the four-terminal perovskite/silicon tandem SC.

4. Conclusion

Spectrally semi-transparent triple-cation perovskite layers have been grown and employed in the four-terminal perovskite/silicon tandem SCs. The corresponding cells have been fabricated basing on the industrial *n*-type monocrystalline bifacial passivated emitter rear totally diffused silicon SC. The experimental studies of the main photovoltaic properties of the separate subcells and the whole four-terminal perovskite/silicon SC have been carried out. The top perovskite cell reveals a good optical transmittance in the wavelength region 750–1100 nm. The PCE of the perovskite subcell amounts to 19.4%. The efficiency of the four-terminal perovskite/silicon SC is equal to 26.6%, which is higher than the individual efficiencies of the separate cells.

References

1. Yu C, Xu S, Yao J and Han S, 2018. Recent advances in and new perspectives on crystalline silicon solar cells with carrier-selective passivation contacts. Crystals. **8**: 430–41.

2. Andreani L C, Bozzola A, Kowalczewski P, Liscidini M and Redorici L, 2019. Silicon solar cells: toward the efficiency limits. Adv. Phys. **4**: 1548305.

3. Węgierek P, Pastuszak J, Dziadosz K and Turek M, 2020. Influence of substrate type and dose of implanted ions on the electrical parameters of silicon in terms of improving the efficiency of photovoltaic cells. Energies. **13**: 6708.

4. Tiedje T, Yablonovitch E, Cody G D and Brooks B G, 1984. Limiting efficiency of silicon solar cells. IEEE Trans. Electron. Devices. **31**: 711–716.

5. Ašmontas S, Gradauskas J, Sužiedėlis A, Šilėnas A, Širmulis E, Vaičikauskas V, Vaičiūnas V, Žalys O, Fedorenko L and Bulat L, 2016. Photovoltage formation across GaAs p-n junction under illumination of intense laser radiation. Opt. Quant. Electron. **48**: 448.

6. Ašmontas S, Gradauskas J, Sužiedėlis A, Šilėnas A, Širmulis E, Švedas V, Vaičikauskas V, Vaičiūnas V, Žalys O and Kostylyov V, 2017. Photovoltage formation across Si p-n junction exposed to laser radiation. Mater. Sci. – Poland. **36**: 337–340.

7. Ašmontas S, Gradauskas J, Sužiedėlis A, Šilėnas A, Širmulis E, Švedas V, Vaičikauskas V and Žalys O, 2018. Hot carrier impact on photovoltage formation in solar cells. Appl. Phys. Lett. **113**: 071103.

8. Ašmontas S, Fedorenko L, Vlasiuk V, Gorbanyuk T, Kostylyov V, Lytovchenko V, Gradauskas J, Sužiedėlis A, Širmulis E, Žalys O and Masalskyi O, 2020. Suppression of hot carriers by nanoporous silicon for improved operation of a solar cell. Ukr. J. Phys. Opt. **21**: 207–214.

9. Ašmontas S, Čerškus A, Gradauskas J, Grigucevičienė A, Leinartas K, Lučun A, Petrauskas K, Selskis A, Sužiedėlis A, Širmulis E and Juškėnas R, 2021. Cesium-containing triple cation perovskite solar cells. Coatings. **11**: 279.

10. Albrecht S, Saliba M, Baena J P C, Lang F, Kegelmann L, Mews M, Steier L, Abate A, Rappich J, Korte L, Schlatmann R, Nazeeruddin M K, Hagfeldt A, Grätzel M and Rech B, 2015. Monolithic perovskite/silicon-heterojunction tandem solar cells processed at low temperature. Energy Environ. Sci. **9**: 81–88.

11. McMeekin D P, Sadoughi G, Rehman W, Eperon G E, Saliba M, Hörantner M T, Haghighirad A, Sakai N, Korte L, Rech B, Johnston M B, Herz L M, Snaith H J and 2016. A mixed-cation lead mixed-halide perovskite absorber for tandem solar cells. Science. **351**: 151–155.

12. Werner J, Niesen B and Ballif C, 2017. Perovskite/silicon tandem solar cells: marriage of convenience or true love story? – An overview. Adv. Matter. **5**: Interf. 1700731.

13. Chen B, Yu Z, Liu K, Zheng X, Liu Y, Shi J, Spronk D, Rudd P N, Holman Z and Huang J, 2019. Grain engineering for perovskite/silicon monolithic tandem solar cells with efficiency of 25.4%. Joule. **3**: 1–14.

14. Shen H, Walter D, Wu Y, Fong K C, Jacobs D A, Duong T, Peng J, Weber K, White T P and Catchpole K R, 2019. Monolithic perovskite/Si tandem solar cell: pathways to over 30% efficiency. Adv. Energy Mater. **10**: 1902840.

15. Ho-Baillie A W Y, Zheng J, Mahmud M A, Ma F-J, McKenzie D R and Green M A, 2021. Recent progress and future prospects of perovskite solar cells. Appl. Phys. Rev. **8**: 041307.

16. Yuan J, Huang T, Cheng P, Zou Y, Zhang H, Yang J L, Chang S Y, Zhang Z, Huang W, Wang R, Meng D, Gao F and Yang Y, 2019. Enabling low voltage losses and high photocurrent in fullerene-free organic photovoltaics. Nature Commun. **10**: 570.

17. Sahli F, Werner J, Kamino B A, Bräuninger M, Monnard R, Paviet-Salomon B, Barraud L, Ding L, Leon J J D, Sacchetto D et al., 2018. Fully textured monolithic perovskite/silicon tandem solar cells with 25.2% power conversion efficiency. Nature Mater. **17**: 820–826.

18. Polman A, Knight M, Garnett E C, Ehrler B and Sinke W C, 2016. Photovoltaic materials: present efficiencies and future challenges. Science. **352**: aad4424-1-aad442-10.

19. Jaysankar M, Filipič M, Zielenski B, Schmager R, Song W, Qiu W, Paetzold U W, Aernouts T, Debucquoy M, Gehlhaar R and Poortmans J, 2018. Perovskite-silicon tandem solar modules with optimized light harvesting. Energy Environ. Sci. **11**: 1489–1498.

20. Charibzadeh S, Hossain I M, Fassl P, Nejand B A, Abzieher T, Schultes M, Ahlswede E, Jackson P, Powalla M, Schäfer S, Rienäcker M, Wietler T, Peibst R, Lemmer U, Richards B S and Paetzold U W, 2020. 2D/3D heterostructure for semitransporant perovskite solar cell with engineering badgap enables efficiencies exceeding 25% in four-terminal tandems with silicon and CIGS. Adv. Funct. Mater. **30**: 1909919.

21. Yeom K M, Kim S U, Woo M Y, Noh J H and Im S H, 2020. Recent progress in metal halide perovskite-based tandem solar cell. Adv. Mater. **32**: 2002228.

22. De Wolf S, Holovsky J, Moon S-J, Löper P, Niesen B, Ledinsky M, Haug F-J, Yum J-H and Ballif C, 2014. Organometallic halide perovskites: sharp optical absorption edge and its relation to photovoltaic performance. J. Phys. Chem. Lett. **5**: 1035–1039.

23. Wehrenfennig C, Eperon G E, Johnston M B, Snaith H J and Herz L M, 2014. High carrier mobilities and lifetimes in organolead trihalide perovskites. Adv. Mater. **26**: 1584–11589.

24. Karakus M, Jensen S A, D´Angelo F, Turchinovich D, Bonn M and Cánovas E, 2015. Phonon-electron scattering limits free charge mobility in methylammonium lead iodide perovskites. J. Phys. Chem. Lett. **6**: 4991–4996.

25. Stranks S D, Eperon G E, Grancini G, Menelaou C, Alcocer M J P, Leijtens T, Herz L M, Petrozza A and Snaith H J, 2013. Electron-hole diffusion lengths exceeding 1 micrometer in an organometal trihalide perovskite absorber. Science. **342**: 341–344.

26. Kothandaraman R K, Jiang Y, Feurer T, Tiwari A N and Fu F, 2020 Near-infrared-transparent perovskite solar cells and perovskite-based tandem photovoltaics. Small Methods. **4**: 2000395.

27. Staub F, Hempel H, Hebig J-C, Mock J, Paetzold U W, Rau U, Unold T and Kirchartz T, 2016. Beyond bulk lifetimes: insights into lead halide perovskite films from time-resolved photoluminescence. Phys. Rev. Appl. **6**: 044017.

28. Solanki A, Yadav P, Turren-Cruz S-H, Lim S S, Saliba M and Sum T C, 2019. Cation influence on carrier dynamics in perovskite solar cells. Nano Energy. **58**: 604–611.

29. Saliba M, Matsui T, Seo J Y, Domaski K, Correa-Baena J P, Nazeeruddin M K, Zakeeruddin S M, Tress W, Abate A, Hagfeldt A and Grätzel M, 2016. Cesium-containing triple cation perovskite solar cells: improved stability, reproducibility and high efficiency. Energy Environ. Sci. **9**: 1989–1997.

30. Singh T and Miyasaka T, 2018. Stabilizing the efficiency beyond 20% with the mixed cation perovskite solar cell fabricated in ambient air under controlled humidity. Adv. Energy Mater. **8**: 1700677.

31. Domanski K, Alharbi E A, Hagfeldt A, Grätzel M and Tress W, 2018. Systematic investigation of the impact of operation conditions on the degradation behaviour of perovskite solar cells. Nature Energy. **3**: 61–67.

32. Wang J, Zou X, Zhu J, Cheng J, Chen D, Bai X, Yao Y, Chang C, Yu X, Liu B, Zhou Z and Li G, 2020. Effect of optimization of TiO_2 electron transport layer on performance of perovskite solar cells with rough FTO substrates. Materials. **13**: 2272.

33. Ašmontas S, Čerškus A, Gradauskas J, Grigucevičienė A, Juškėnas R, Leinartas K, Lučun A, Petrauskas K, Selskis A, Staišiūnas L, Sužiedėlis A, Šilėnas A and Širmulis E, 2022. Photoelectric properties of planar and mesoporous structured perovskite solar cells. Materials. **15**: 4300.

34. Mazarella L, Lin Y H, Kirner S, Morales-Vilches A B, Korte L, Albrecht S, Crossland E, Stannowski B, Case C, Snaith H J and Schlatmann R, 2019. Infrared light management using a nanocrystalline silicon oxide interlayer in monolithic perovskite/silicon heterojunction tandem solar cells with efficiency above 25%. Adv. Energy Mater. **9**: 1803241.

35. Samantaray M R, Ghosh D S and Chander N, 2022, Four-terminal perovskite/silicon tandem solar cells based on large-area perovskite solar cells utilizing low-cost copper semi-transparent electrode. Appl. Phys. A. **128**: 111.

Анотація. *Тандемний сонячний елемент, який складається з перовскитового елементу, поміщеного поверх кремнієвого елементу, є багатообіцяючим варіантом для перевищення межі Шоклі–Квайссера для одноперехідних сонячних елементів. Ми дослідили фотоелектричні властивості трикатіонного чотиритермінального тандемного перовскит/кремнієвого сонячного елемента, який складається з перовскитового елемента на основі напівпрозорого шару $Cs_{0.06}(MA_{0.17}FA_{0.83})_{0.94}Pb(I_{0.83}Br_{0.17})_3$, розміщеного на промисловому кремнієвому монокристалічному двосторонньому сонячному елементі PERT n-типу. Досягнута нами ефективність перетворення енергії у 26.6% є одним із найвищих значень, зареєстрованих для чотиритермінальних тандемних перовскит/кремнієвих сонячних елементів.*